




A SAR speckle filter based on Residual Convolutional Neural Networks

Alessandro Sebastianelli , *Member, IEEE* *, Maria Pia Del Rosso , *Member, IEEE* *,
Silvia L. Ullo , *Senior Member, IEEE* *

Abstract—In recent years, Machine Learning (ML) algorithms have become widespread in all fields of Remote Sensing (RS) and Earth Observation (EO). This has allowed a rapid development of new procedures to solve problems affecting these sectors. In this context, the authors of this work aim to present a novel method for filtering the speckle noise from Sentinel-1 data by applying Deep Learning (DL) algorithms, based on Convolutional Neural Networks (CNNs). The obtained results, if compared with the state of the art, show a clear improvement in terms of Peak Signal-to-Noise Ratio (PSNR) and Structural Similarity Index (SSIM), by proving the effectiveness of the proposed architecture. Moreover, the generated open-source code and dataset have been made available for further developments and investigation by interested researchers.

Index Terms—Synthetic Aperture Radar (SAR), Sentinel-1, noise filtering, speckle filtering, Artificial Intelligence (AI), Deep Learning (DL), Convolutional Neural Networks (CNNs).

I. INTRODUCTION

As well known, Synthetic Aperture Radar (SAR) data are affected by several types of noise, and among them, the speckle noise, resulting into a positive or negative interference phenomenon that occurs in each resolution cell. Speckle confers to SAR data a granular aspect, resulting into a high degradation of the image quality [1], unlike optical data, that are characterized by clear and recognizable features. An example of two different images based on SAR data (with speckle) and optical data is shown in Figure 1, where it is evident how the speckle presence prejudices the visual analysis and interpretation of the Area of Interest (AOI). Moreover, speckle also affects the phase of scattering coefficients for the analyzed surface and degrades the signal polarimetric information [2]. Speckle results in misclassification errors and in many other problems if SAR data are not correctly pre-processed.

Classical speckle filtering techniques can be divided into two macro categories: 1) single product speckle filtering, 2) multi-temporal speckle filtering.

Single product speckle filtering methods are mainly based on mathematical models of the speckle phenomenon, and a classic approach in this category is the multilooking, a process that can reduce the speckle by means of incoherent averaging of many sub-aperture acquisitions (looks). This process normally includes the sub-sampling of data and the ground-projection, leading to the increase of the radiometric resolution



(a) Sentinel-1A acquisition on 2021-01-01 focusing on Rome (Italy), Interferometric Wide Swath (IW) mode, Single Look Complex (SLC) data, VV polarization (Intensity).



(b) Sentinel-2A acquisition on 2021-01-01 focusing on Rome (Italy), B4, B3 and B2 bands (RGB channels).

Fig. 1: Comparison between Sentinel-1 (SAR) and Sentinel-2 (optical) acquisitions.

*The authors are with the Department of Engineering, University of Sannio, Benevento, Italy. A. Sebastianelli (email: sebastianelli@unisannio.it), M. P. Del Rosso (email: mpdelrosso@unisannio.it) and S. L. Ullo (email: ullo@unisannio.it).

and the decrease of the spatial one. Yet, after this process the phase information is lost [3]. Another typical approach in the single product speckle filtering category involves the use

of adaptive and non-adaptive filters, the first ones, including the Lee, the Frost, and the Refined Gamma Maximum-A-Posteriori (RGMAP), are better at preserving edges and details in high-texture areas (e.g. urban areas); the second ones are simpler to implement and require less computational power. However, these types of filters can degrade the acquisition and can bring to information loss [4]–[6].

The second category of speckle filtering techniques are based on the multi-temporal filtering approach, that is applied on a dataset of co-registered acquisitions. This approach allows to achieve very high signal-to-noise ratio without degrading the spatial resolution too much [7].

In recent years, the enormous spread of AI-based methods for EO has given rise to the development of speckle filtering techniques, completely new with respect to the traditional ones. They are based on the use of DL algorithms, in particular on CNNs [8]–[11].

II. DATA AND METHODS

The method proposed in this letter involves the use of ML algorithms, more specifically a DL model based on CNNs [12]–[14]. The related network can be classified as a hybrid method since it can be considered as a multi-temporal speckle filter, because the training dataset is composed of a time-series of Sentinel-1 data, and also it can be compared to the Lee filter, commonly used in single product speckle filtering approaches. In fact, similarly to the Lee filter, that proposes an additive model for the speckle noise (by converting the initial multiplicative speckle noise present in the SAR data) [15], the proposed architecture deals with the speckle by subtracting it from the noisy input image.

It is worth to highlight that both the dataset and the model have been developed from scratch and made available for further analysis and investigation on Git-Hub [16], [17].

The approach here proposed is fully based on real SAR data, belonging to a dataset created for this scope, while in other works available in the literature the models were trained on simulated data [11], [9]. Furthermore, the proposed network has shown to achieve better performances than other models based on subtractive methods or based on different models such as for instance the logarithmic state space transform or the divisional layers [8], [9], [11], [18]–[20].

In the following sections both the dataset used and the proposed model will be presented and explained in details, also showing the achieved results and the comparisons with the state of the art.

A. Dataset

Let $\mathbf{X}_{lat,lon} \in \mathbb{R}^{W \times H \times P}$ be a single Sentinel-1 SAR acquisition, with a width W , a height H and a specific polarization P , acquired in the geographical region defined by latitude lat and longitude lon . Through the tool proposed in [21], a time-series of Sentinel-1 acquisitions $\vec{\mathbf{X}}_{lat,lon} \in \mathbb{R}^{T \times W \times H \times P}$ has been downloaded, where T denotes the length of the time-series.

Data have been collected from the Google Earth Engine catalog [22], containing the full Sentinel-1 archive of GRD (Ground Ranged Detected) products. GRD data consist of focused SAR data that have been detected, multi-looked and projected to ground range using an Earth ellipsoid model. Phase information is lost. This product has approximately square spatial resolution pixels spacing with reduced speckle at the cost of lower spatial resolution [23].

Since the proposed method for filtering the SAR speckle is based on CNNs, trained in a supervised way, both the input and the expected output (ground truth) should be available for the model training. In this case, the ground truth is a Sentinel-1 acquisition with the lowest possible speckle influence. It has been obtained by a temporal average of $\vec{\mathbf{X}}_{lat,lon}$, as expressed by the equation:

$$\mathbf{X}_{lat,lon}^* = \frac{1}{T} \sum_{t=1}^T \vec{\mathbf{X}}_{lat,lon}^t, \quad \mathbf{X}_{lat,lon}^* \in \mathbb{R}^{W \times H \times P} \quad (1)$$

while the input has been obtained by adding to the ground truth $\mathbf{X}_{lat,lon}^*$ the speckle \mathbf{S} , generated through a statistical representation based on a Rayleigh distribution $R \sim \text{Rayleigh}(\sigma)$ [24]. The generated speckle has the same dimensions of the ground truth, $\mathbf{R} \in \mathbb{S}^{W \times H \times P}$. The input image is then derived using the equation:

$$\mathbf{X}_{lat,lon}^s = \mathbf{X}_{lat,lon}^* \times \mathbf{S}, \quad \mathbf{X}_{lat,lon}^s \in \mathbb{R}^{W \times H \times P} \quad (2)$$

This process was repeated an arbitrary number of times (this choice will define the size of the final dataset) by randomly selecting latitude lat and longitude lon values, distributed over the land surface.

The inputs and the ground truths are then grouped in vectors, in order to form the dataset as expressed through equations (3a) and (3b).

$$\vec{\mathbf{X}}_{inputs} = [\mathbf{X}_{lat_0,lon_0}^s, \dots, \mathbf{X}_{lat_N,lon_N}^s] \quad (3a)$$

$$\vec{\mathbf{X}}_{ground_truths} = [\mathbf{X}_{lat_0,lon_0}^*, \dots, \mathbf{X}_{lat_N,lon_N}^*] \quad (3b)$$

where $\vec{\mathbf{X}}_{inputs}, \vec{\mathbf{X}}_{ground_truths} \in \mathbb{R}^{N \times W \times H \times P}$, with N representing the number of Sentinel-1 acquisitions on the Earth surface.

Finally, the dataset is divided into two sub-datasets, respectively the training dataset $\vec{\mathbf{X}}_{inputs}^t, \vec{\mathbf{X}}_{ground_truths}^t \in \mathbb{R}^{M \times W \times H \times P}$ and the validation dataset $\vec{\mathbf{X}}_{inputs}^v, \vec{\mathbf{X}}_{ground_truths}^v \in \mathbb{R}^{Q \times W \times H \times P}$, where $M = 80\%$ of N and $Q = 20\%$ of N .

The final dataset contains 3955 Sentinel-1 acquisitions without speckle and 3955 corresponding acquisitions with speckle. Using the training-validation split factor of 20%, as above specified, the resulting training dataset is composed of 3164 samples and the validation dataset of 791 samples. Both datasets are subjected to data augmentation to artificially increase the actual size of the dataset, through transformations of the starting image (e.g. rotation, crops, etc.).

A version of the proposed dataset has been made available online as open access [17].

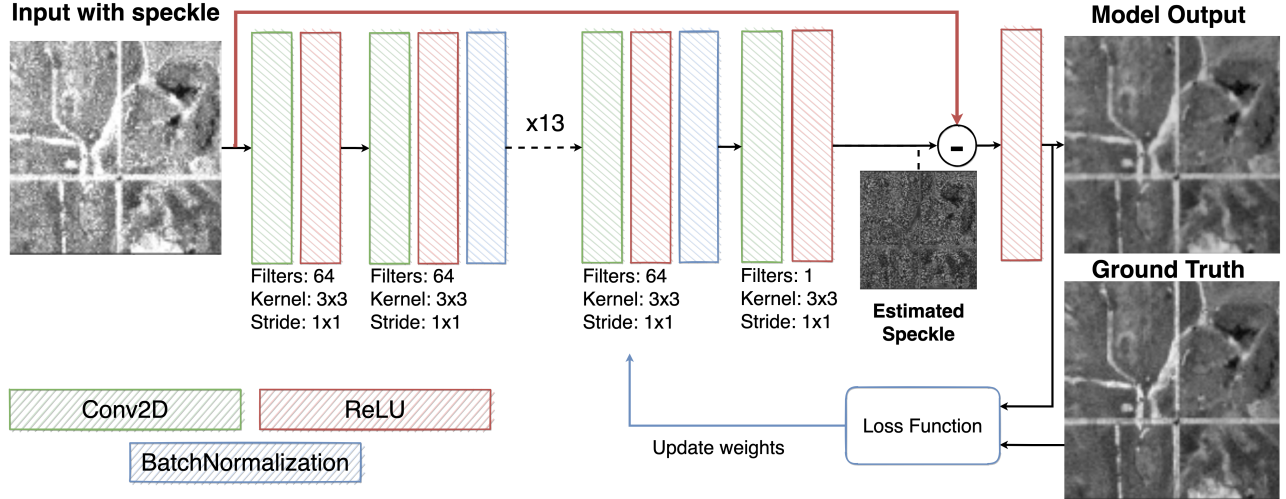


Fig. 2: Proposed model for speckle filtering

B. Proposed approach

The proposed approach is based on the extraction of the speckle from the input Sentinel-1 acquisition through a CNN. The extracted speckle will be then subtracted to the input image through a skip connection, that makes the model also residual, and through a subtraction layer [25]. The output of the subtraction layer will be the filtered Sentinel-1 acquisition.

The model is essentially composed of three components: 1) the CNN, 2) the skip connection and 3) the subtraction layer, as shown in Figure 2. The CNN is composed of repeated fundamental blocks, such as Convolutional 2D, ReLU and Batch Normalization. It mainly deals with the extraction of speckle noise from the input data. The skip connection, the red arrow in Figure 2, which connects the input with the subtraction layer, is essentially a connection used to skip the CNN. The subtraction layer applies the mathematical subtraction between the input data, through the skip connection and the CNN output. The result, after the last ReLU layer, is the filtered Sentinel-1 acquisition.

During the training of the model, lasting 50 epochs, a batch of 16 Sentinel-1 acquisitions from the training dataset $\tilde{\mathbf{X}}_{inputs}^t$ is used as feedforward input for the model. The predicted images $\mathbf{Y} \in \mathbb{R}^{W \times H \times P}$ are compared with the corresponding ground truths acquisition from the training dataset $\tilde{\mathbf{X}}_{ground_truths}^t$, through the Mean Absolute Error loss function. Using this loss function and its gradient, the Adam optimizer [26] updates the weights of the network, with a learning rate of 0.0001.

Before the training, both the input and the expected output have been normalized into the range $[0, 1]$ using the min-max normalization formula (4). Data normalization is a very common technique in ML and it allows the model to learn faster and to produce better results [27].

$$\mathbf{Y} = \frac{\mathbf{X} - \min}{(\max - \min) + \varepsilon} \quad (4)$$

In Equation (4), \mathbf{X} represents the image to be normalized, \min and \max are the minimum and the maximum values computed on the overall dataset, ε is set to $1 \cdot 10^{-6}$ and it is used to stabilize the division with a weak denominator and \mathbf{Y} is the normalized image. The minimum and the maximum values have been computed on the overall dataset in order to restore the range of the model output using the inverse formula given by:

$$\mathbf{Y} = \mathbf{X}(\max - \min)\varepsilon + \min \quad (5)$$

In Equation (5), \mathbf{X} represents the model output to be restored, \mathbf{Y} is the restored image and \min , \max and ε are the variables mentioned above.

The model has been developed in *Tensorflow-Keras* and has been trained on the freely available GPUs of the platform Google Colaboratory [28]. The code has been made available and can be found at [16] for further analysis and experiments.

III. RESULTS AND DISCUSSION

The model has been tested on the validation dataset $\tilde{\mathbf{X}}_{inputs}^v, \tilde{\mathbf{X}}_{ground_truths}^v$, through two different metrics, the *PSNR* and the *SSIM* [29].

The *PSNR*, in this case, gives a measure of the filtering process quality. It is the ratio between the maximum power of the ground truth acquisition and the residual error between the ground truth and the acquisition filtered by the model, and it is computed using the equation:

$$\begin{aligned} \text{PSNR}(\mathbf{x}_{inputs}^v, \mathbf{x}_{ground_truths}^v) &= \\ &= 10 \log_{10} \left(\frac{\max(\mathbf{x}_{ground_truths}^v)^2}{\|\mathbf{x}_{ground_truths}^v - \mathbf{x}_{inputs}^v\|_2^2 / N} \right) \quad (6) \end{aligned}$$

The *SSIM* measures the similarity between two acquisitions. It is a perception-based model that considers the image degradation as perceived change in the structural information. Let \mathbf{x} be an input acquisition taken from the validation dataset $\tilde{\mathbf{X}}_{inputs}^v$ and let \mathbf{y} be a ground truth acquisition taken from the

validation dataset $\vec{X}_{ground_truths}^v$, then the *SSIM* is computed by using the equation:

$$SSIM(x, y) = \frac{(2\mu_x\mu_y + c_1)(2\sigma_{xy} + c_2)}{(\mu_x^2 + \mu_y^2 + c_1)(\sigma_x^2 + \sigma_y^2 + c_2)} \quad (7)$$

where μ_x is the average of \mathbf{x} , μ_y is the average of \mathbf{y} , σ_x^2 is the variance of \mathbf{x} , σ_y^2 is the variance of \mathbf{y} , σ_{xy}^2 is the covariance of \mathbf{x} and \mathbf{y} , $c_1 = (k_1L)^2$ and $c_2 = (k_2L)^2$ are two variables that stabilize the division with a weak denominator, L is the dynamic range of the pixel-values (typical $2^{\#BitsPerPixel} - 1$), $k_1 = 0.01$ and $k_2 = 0.03$ by default.

Qualitative results are presented in Figure 3, where each row represents a different acquisition. For each test there are four images representing: 1) the estimated speckle, 2) the input acquisition with speckle, 3) the model output and 4) the ground truth. Each test has shown that the model can produce an output comparable to the ground truth.

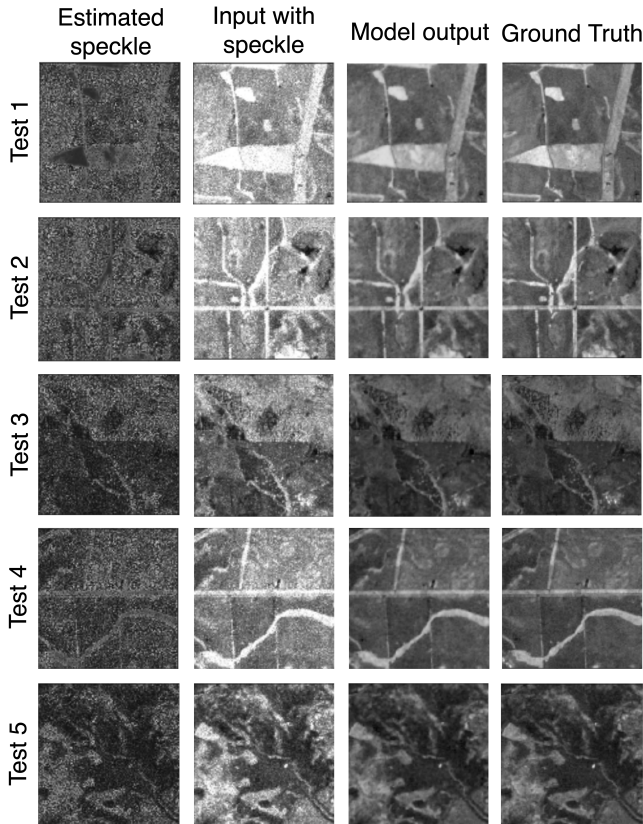


Fig. 3: Model evaluation on validation dataset

Quantitative results, related to Figure 3, have been reported in Table I, demonstrating that the model is able to restore speckle-corrupted data. Note that the *SSIM* ranges from 0 to 1, where 1 is the best/ideal value and for the *PSNR*, that is a signal to noise ratio, the greater the value the better the result, the ideal value is $+\infty$. Table I is structured in five rows representing the different tests, each row containing both *PSNR* and *SSIM* results computed for input with speckle versus ground truth and input with speckle versus model output. The results obtained are very promising, especially when compared to classical methods available in the state of

Test	Metric	Input with speckle	Model Output
Test 1	PSNR	17.93 dB	31.81 dB
Test 1	SSIM	0.37	0.91
Test 2	PSNR	10.28 dB	25.79 dB
Test 2	SSIM	0.38	0.79
Test 3	PSNR	17.07 dB	31.94 dB
Test 3	SSIM	0.31	0.90
Test 4	PSNR	17.46 dB	31.53 dB
Test 4	SSIM	0.36	0.80
Test 5	PSNR	12.64 dB	28.34 dB
Test 5	SSIM	0.36	0.81

TABLE I: Models scores on a sample of the validation dataset

the art. With this regard, in Table II a comparison with the state of the art is presented, the proposed method leads to higher performances than the other approaches in terms of *PSNR* and *SSIM* [8], [9], [18]–[20]. Table II is structured in three blocks: 1) metrics computed on the input data with speckle, 2) metrics computed on filtered data using classic methods and 3) metrics computed on filtered data using machine learning methods.

Model	PSNR	SSIM
Input	14.53 dB	0.369
Lee	21.48 dB	0.511
Kuan	21.95 dB	0.592
PPB	21.74 dB	0.619
SAR-BM3D [18]	22.99 dB	0.692
CNN [19], [20]	21.04 dB	0.631
SAR-CNN [8]	23.59 dB	0.641
ID-CNN [9]	24.74 dB	0.727
Proposed Model	28.83 dB	0.843

TABLE II: Comparisons with the state of the art: first block input, second block classical methods, third block machine learning based methods.

IV. CONCLUSIONS

In this letter, a method for SAR speckle filtering, based on Convolutional Neural Networks, has been presented and discussed. Both the dataset and the model have been developed from scratch and made available for further analysis and investigation on Git-Hub. Both qualitative and quantitative results have been shown to prove the effectiveness of the proposed architecture. The results obtained are very promising, especially if compared with the ones found in the state of the art.

The architecture presented can obviously be improved through a tuning of the hyperparameters, an optimal selection of number of layers and the implementation of a proper loss function, that will help in reducing both the amount of noise and the image blurring. Among the future developments, there could be the integration of a much more complex speckle model, adaptable to the typology of the Earth surface contained in each acquisition. Furthermore, the model could be trained

on a dataset containing images with speckle at different power, in order to make it more robust [30].

A further future development consists in the application of the model to Sentinel-1 SLC data, with the aim of integrating the CNNs-based filter into SAR data processing pipelines that also involve phase information (e.g. interferometry [31]).

REFERENCES

- [1] J. W. Goodman, "Some fundamental properties of speckle," *JOSA*, vol. 66, no. 11, pp. 1145–1150, 1976.
- [2] C. López-Martínez and X. Fabregas, "Polarimetric sar speckle noise model," *IEEE Transactions on Geoscience and Remote Sensing*, vol. 41, no. 10, pp. 2232–2242, 2003.
- [3] C. Oliver and S. Quegan, *Understanding synthetic aperture radar images*. SciTech Publishing, 2004.
- [4] S. Banerjee, S. S. Chaudhuri, R. Mehra, and A. Misra, "A survey on lee filter and its improved variants," in *Advances in Smart Communication Technology and Information Processing: OPTRONIX 2020*. Springer Singapore, 2021, pp. 371–383.
- [5] A. Baraldi and F. Parmiggiani, "A refined gamma map sar speckle filter with improved geometrical adaptivity," *IEEE Transactions on Geoscience and Remote Sensing*, vol. 33, no. 5, pp. 1245–1257, 1995.
- [6] J.-S. Lee, "Speckle suppression and analysis for synthetic aperture radar images," *Optical engineering*, vol. 25, no. 5, p. 255636, 1986.
- [7] S. Quegan, T. L. Toan, J. J. Yu, F. Ribbes, and N. Floury, "Multitemporal sar analysis applied to forest mapping," *IEEE Transactions on geoscience and remote sensing*, vol. 38, no. 2, pp. 741–753, 2000.
- [8] G. Chierchia, D. Cozzolino, G. Poggi, and L. Verdoliva, "Sar image despeckling through convolutional neural networks," in *2017 IEEE International Geoscience and Remote Sensing Symposium (IGARSS)*, 2017, pp. 5438–5441.
- [9] P. Wang, H. Zhang, and V. M. Patel, "Sar image despeckling using a convolutional neural network," *IEEE Signal Processing Letters*, vol. 24, no. 12, pp. 1763–1767, 2017.
- [10] P. Wang and V. M. Patel, "Generating high quality visible images from sar images using cnns," in *2018 IEEE Radar Conference (RadarConf18)*. IEEE, 2018, pp. 0570–0575.
- [11] F. Lattari, B. Gonzalez Leon, F. Asaro, A. Rucci, C. Prati, and M. Matteucci, "Deep learning for sar image despeckling," *Remote Sensing*, vol. 11, no. 13, p. 1532, 2019.
- [12] I. Goodfellow, Y. Bengio, A. Courville, and Y. Bengio, *Deep learning*. MIT press Cambridge, 2016, vol. 1, no. 2.
- [13] Y. LeCun, Y. Bengio, and G. Hinton, "Deep learning," *nature*, vol. 521, no. 7553, pp. 436–444, 2015.
- [14] P. Kim, "Convolutional neural network," in *MATLAB deep learning*. Springer, 2017, pp. 121–147.
- [15] L. Gagnon and A. Jouan, "Speckle filtering of sar images: a comparative study between complex-wavelet-based and standard filters," in *Wavelet Applications in Signal and Image Processing V*, vol. 3169. International Society for Optics and Photonics, 1997, pp. 80–91.
- [16] A. Sebastianelli, M. Del Rosso, and S. L. Ullo, "CNN Speckled Filter Git-Hub repository," <https://github.com/Sebbyraft/CNNSpeckleFilter>.
- [17] ———, "Sentinel-1 GRD dataset: Git-Hub repository," https://github.com/Sebbyraft/sentinel_1_GRD_dataset.
- [18] S. Parrilli, M. Poderico, C. V. Angelino, and L. Verdoliva, "A nonlocal sar image denoising algorithm based on lmmse wavelet shrinkage," *IEEE Transactions on Geoscience and Remote Sensing*, vol. 50, no. 2, pp. 606–616, 2011.
- [19] J. M. Bioucas-Dias and M. A. Figueiredo, "Multiplicative noise removal using variable splitting and constrained optimization," *IEEE Transactions on Image Processing*, vol. 19, no. 7, pp. 1720–1730, 2010.
- [20] K. Zhang, W. Zuo, Y. Chen, D. Meng, and L. Zhang, "Beyond a gaussian denoiser: Residual learning of deep cnn for image denoising," *IEEE transactions on image processing*, vol. 26, no. 7, pp. 3142–3155, 2017.
- [21] A. Sebastianelli, M. P. Del Rosso, and S. L. Ullo, "Automatic dataset builder for machine learning applications to satellite imagery," *arXiv preprint arXiv:2008.01578*, 2020.
- [22] N. Gorelick, M. Hancher, M. Dixon, S. Ilyushchenko, D. Thau, and R. Moore, "Google earth engine: Planetary-scale geospatial analysis for everyone," *Remote Sensing of Environment*, 2017. [Online]. Available: <https://doi.org/10.1016/j.rse.2017.06.031>
- [23] The European Space Agency, "Sentinel-1 data products," 2021, online; accessed 18 January 2021.
- [24] E. E. Kuruoglu and J. Zerubia, "Modeling sar images with a generalization of the rayleigh distribution," *IEEE Transactions on Image Processing*, vol. 13, no. 4, pp. 527–533, 2004.
- [25] Del Rosso, Maria Pia and Sebastianelli, Alessandro and Ullo, Silvia Liberata, *Artificial Intelligence Applied to Satellite-based Remote Sensing Data for Earth Observation*. Book under contract with a scheduled publication of spring/summer2021. IET (Institute of Engineering and Technology) Digital Library, 2021.
- [26] Z. Zhang, "Improved adam optimizer for deep neural networks," in *2018 IEEE/ACM 26th International Symposium on Quality of Service (IWQoS)*. IEEE, 2018, pp. 1–2.
- [27] D. Singh and B. Singh, "Investigating the impact of data normalization on classification performance," *Applied Soft Computing*, vol. 97, p. 105524, 2020.
- [28] E. Bisong, "Google colaboy," in *Building Machine Learning and Deep Learning Models on Google Cloud Platform*. Springer, 2019, pp. 59–64.
- [29] A. Hore and D. Ziou, "Image quality metrics: Psnr vs. ssim," in *2010 20th international conference on pattern recognition*. IEEE, 2010, pp. 2366–2369.
- [30] Z. He, A. S. Rakin, and D. Fan, "Parametric noise injection: Trainable randomness to improve deep neural network robustness against adversarial attack," in *Proceedings of the IEEE/CVF Conference on Computer Vision and Pattern Recognition*, 2019, pp. 588–597.
- [31] T. De Corso, L. Mignone, A. Sebastianelli, M. P. Del Rosso, C. Yost, E. Ciampa, M. Pecce, S. Sica, and S. Ullo, "Application of dinsar technique to high coherence satellite images for strategic infrastructure monitoring," *arXiv preprint arXiv:2004.09501*, 2020.